Modeling a Tri-Axial Gas Puff Valve for use in Pulsed-Power Z-pinches

Benjamin Inbar
Sibley School of Mechanical and Aerospace Engineering, Cornell University, Ithaca, NY 14850

The stability of gas puff Z-pinch plasmas are highly dependent on the radius of the gas column used to generate them. However by using annular gas shells rather than a filled gas column and by carefully tuning the density of each shell, stability can be significantly increased. This paper discusses preliminary work on the development of a computational model of the gas puff valve in the Cornell Beam Research Accelerator in order to better characterize the density profiles. A 2D planar model, and a 2D axisymmetric model have been carried using commercially available computational fluid dynamics (CFD) codes. The results from the two models were then evaluated and compared with experimental data collected through Planar Laser Induced Fluorescence. While neither model showed accurate predictions of experimental data, they establish a clear base from which higher fidelity models can be built.

I. Introduction

The Laboratory of Plasma Studies (LPS) at Cornell University is involved in a wide range of plasma physics research with a focus on pulsed-power machines and high energy density (HED) plasmas. The Cornell Beam Research Accelerator (COBRA) is a versatile pulsed-power machine within LPS, capable of generating a number of HED plasmas including wire array & gas puff Z-pinches, X-pinches and conical wire arrays. Gas puff Z-pinch plasmas produce intense X-rays along with a hot and energetic plasma making them ideal X-ray sources [1]. Gas puff Z-pinches are formed by passing a high current through a column of gas causing breakdown and ionization, the current induces a magnetic field within the column that causes the puff to pinch in on itself towards the z-axis along the center of the column[2]. This implosion heats the compressed plasma and causes it to release energy in the form of radiation before dissipating. These types of plasmas are particularly susceptible to Magneto-Rayleigh-Taylor (MRT) instabilities which for single shell or full column gas pinches grows exponentially with a growth rate proportional to the initial column radius [3]. Introducing multi-shelled gas columns which allow controlled density profiles have been shown to add increased stability to Z-pinch plasmas [3].

While significant advancement has been made in Z-pinch stability through the use of bi and tri-axial gas puffs, that stability is dependent on the ability to carefully control the density of the gas column [3]. While there have been significant experimental attempts to characterize the gas puffs produced for pulsed-power machines such as COBRA, there has been very little computational analysis of these systems. One example of the experimental effort to better understand the gas columns produced in these machines was conducted at Cornell using the Planar Laser Induced Fluorescence (PLIF) technique to image the puff [4]. This experimental work allows for the direct measurement of the particular cases under examination, but does not lend itself to being able to characterize the gas puff at a wide range of plena pressures and firing modes. A computational model would allow the prediction of gas puff behavior over a wide range of initial conditions without the need to run the experiment in those modes. Once established and validated, a computational model could also be used to design puffs that would yield higher stability Z-pinches. This paper discusses the preliminary development of a such a model for the COBRA tri-axial gas puff valve using commercially available computational fluid dynamics codes. Two simplified models of the COBRA tri-axial gas puff valve were developed, a 2D planar model and a 2D axisymmetric model. These models are working towards a higher fidelity model of the valve in the future.

II. Numerical methods

A. Pressure-based Solver

The simulation of the gas puff valve has been carried out in ANSYS Fluent, a commercially available closed-source CFD code widely used in industry. Because of this, it is not possible to determine the exact methods it is applying

in order to solve a particular problem. The software gives users the choice between either a Pressure-based or a Density-based solver. Both solvers are suitable to a wide range of flow regimes including high-speed compressible flow, however, the Density-based solver was initially developed to provide higher quality simulations of compressible flow [5].

Unfortunately the Density-based solver included with ANSYS Fluent is newer and less well developed than the Pressure-based solver and so early attempts to model the system using it resulted in highly inaccurate results. After consulting with Professor Rajesh Bhaskaran, the Swanson Director for Engineering Simulation at Cornell University, the simulation was changed to utilize the Pressure-based solver which is more stable than the Density solver.

The Pressure-based solver uses a sequential algorithm for solving the simulation's governing equations. In this algorithm each governing equation is solved sequentially, to obtain a solution for that particular iteration. The solver takes the results of the previous iteration and solves the Momentum equations sequentially using those values. It then uses the generated velocity field to solve the pressure correction equation which is then applied to the calculated quantities for this iteration. It then solves for turbulence using the specified turbulence model, energy, and species transport. Once these equations have been solved, the solver checks for convergence between this iteration and the previous. If the convergence criteria is met, the solver steps to the next timestep, if not the solver takes the final solutions and applies them to the next iteration [6]. The equations that are being solved by the Pressure-based solver are presented in Sec. II.B

B. Governing Equations

The fluid flow being investigated in this simulation is governed by three main equations, Mass conservation or the Continuity equation, the Momentum Conservation equation, and the Energy Equation. The derivative forms of these equations are presented in this section, however ANSYS Fluent applies the integral form of these equations in order to solve flow problems [6]. This means that while the presented governing equations hold point wise over the domain, the final integral form that is solved only holds in an average sense over that same domain. Additionally the equations presented in this section are formulated in cartesian reference frame most easily applicable to the 2D planar however these equations can be reformulated to apply to the axisymmetric coordinate system easily.

Conservation of Mass is given in the following equation. This formulation allows for changing density making it applicable to compressible flows.

$$\frac{\partial \rho}{\partial t} + \nabla \cdot (p\vec{v}) = S_m \tag{1}$$

In this equation ρ is the fluid density, p is the pressure and $\vec{v}$ is the velocity vector. The S_m term allows for the possibility of either a mass source or sink, however the particular case investigated here has no source/sink and so this term is 0.

Conservation of Momentum is governed by the Navier-Stokes equation (Eqn. 2). The terms on the right hand side of the equation represent the pressure gradient, viscous forces and external forces on the fluid.

$$\frac{\partial}{\partial t}(\rho\vec{v}) + \nabla \cdot (\rho\vec{v}\vec{v}) = -\nabla p + \nabla \cdot \bar{\bar{\tau}} + \rho\vec{g} + \vec{F} \tag{2}$$

The stress tensor $\bar{\bar{\tau}}$ is given by:

$$\bar{\bar{\tau}} = \mu \left[(\nabla\vec{v} + \nabla\vec{v}^T) - \frac{2}{3}\nabla \cdot \vec{v} I \right] \tag{3}$$

Where μ is molecular viscosity and I is the identity matrix.

The final governing equation is the energy equation given in Eqn. 4.

$$\frac{\partial}{\partial t}(\rho(e + \frac{v^2}{2})) + \nabla \cdot (\rho v(h + \frac{v^2}{2})) = \nabla \cdot (k_{eff}\nabla T - \sum_j h_j \vec{J_j} = \bar{\tau_{eff}} \cdot \vec{v}) \tag{4}$$

In this equation k_{eff} represents the sum of the fluid's conductivity and the turbulent conductivity, e is the internal energy, and h_j is the enthalpy of species j. The diffusion flux of species j is given by:

$$\vec{J_j} = -(\rho D_{j,m} + \frac{\mu_t}{Sc_t})\nabla Y_j - D_{T,j}\frac{\nabla T}{T} \tag{5}$$

In Eqn. 5 $D_{j,m}$ is the mass diffusion coefficient for the species j and $D_{T,j}$ is the Thermal diffusion coefficient for species j, and μ_t is the turbulent viscosity [6]. Sc_t is the turbulent Schmidt number which is defined as the ratio between the turbulent viscosity and diffusivity, and can be used to characterize how turbulence is enhancing transport [7].

C. Turbulence Model

It was necessary to choose a Turbulence model for the simulation of the gas puff valve, however determining which model may be the most valid was not necessarily straight forward. ANSYS Fluent recommends the use of the SST $k-\omega$ as the default. This model was used in this simulation due to the better performance $k-\omega$, combined with the reduced sensitivity of the model to the inlet conditions [8].

The $k-\omega$ turbulence model is a general class of two-equation turbulence models that compute an eddy viscosity from the turbulent mixing energy and the specific dissipation rate. The governing equations for the turbulent kinetic energy and specific dissipation rate are shown in Eqn. 6 and Eqn. 7 [9].

$$\frac{\partial}{\partial t}(\rho k) + \frac{\partial}{\partial x_j}(\rho u_j k) = \rho \tau_{ij}\frac{\partial u_i}{\partial x_j} - \beta^* \rho k \omega + \frac{\partial}{\partial x_j}\left[\left(\mu + \sigma^* \frac{\rho k}{\omega}\right)\frac{\partial k}{\partial x_j}\right] \tag{6}$$

$$\frac{\partial}{\partial t}(\rho \omega) + \frac{\partial}{\partial x_j}(\rho u_j \omega) = \alpha \frac{\omega}{k}\rho \tau_{ij} - \beta \rho \omega^2 + \sigma_d \frac{\rho}{\omega}\frac{\partial k}{\partial x_j}\frac{\partial \omega}{\partial x_j} + \frac{\partial}{\partial x_j}\left[\left(\mu + \sigma \frac{\rho k}{\omega}\right)\frac{\partial \omega}{\partial x_j}\right] \tag{7}$$

Where $\alpha, \beta, \beta^*, \sigma, \sigma^*, \sigma_d$ are closure coefficents in their respective equations, x_i is the i component of the position vector, u_i is the i component of averaged velocity vector and τ_{ij} is the specific Reynolds Stress Tensor.

Solving Eqn. 6 and Eqn. 7 for k and ω allows the computation of the eddy viscosity from Eqn. 8, and then the Reynolds stress tensor from the viscosity in Eqn. 9 [9, 10]. This Reynolds stress is then applied to the over all momentum conservation allowing it to incorporate the effects of turbulence.

$$\mu_T = \frac{\rho * k}{\omega} \tag{8}$$

$$\rho \tau_{ij} = \mu_t \left[\frac{\partial u_i}{\partial x_j} + \frac{\partial u_j}{\partial x_i} - \frac{2}{3}\frac{\partial u_k}{\partial x_k}\delta_{ij}\right] - \frac{2}{3}\rho k \delta_{ij} \tag{9}$$

Where δ_{ij} is the Kronecker delta function, and u_i, u_j and u_k are averaged velocity components in the i, j and k unit directions.

The SST formulation of the $k-\omega$ turbulence model was created in order to address the sensitivity that the original model has to the initial freestream velocity and additionally incorporates the effect of principle shear stress transport [11]. This slightly modifies the equations presented to include a $\frac{D\tau}{Dt}$ term to account for the transport of the shear stress, it also modifies the ω equation in order to achieve the reduced sensitivity to the freestream [11].

D. Species Transport

An assumption was made that any gas remaining in the vacuum chamber after pump down would be air, and that the only Argon entering the chamber would be due to the gas puff. This assumption enables the differentiation of the fluid in the chamber at t = 0 from the fluid added to the chamber via the valve. In order to implement this assumption, the Fluent species transport model was adopted.

Fluent calculates the local mass fraction Y_i of each species in a predefined mixture using the convection & diffusion equation shown in Eqn. 10. Fluent solves this equation for n-1 species in the mixture (where n is the total number of species) and the n^{th} species mass fraction is the remainder [6]. Argon was taken to be the n^{th} species because it is anticipated to have the highest overall mass fraction.

$$\frac{\partial}{\partial t}(\rho_i Y_i) + \nabla \cdot (\rho \vec{v}\, Y_i) = -\nabla \cdot \vec{J}_i + S_i \tag{10}$$

Here ρ_i is the density of species i, $\vec{v}$ is the local velocity vector, and S_i is a source term for species i. Eqn. 10 is also dependent on the diffusive flux of species i, which for turbulent flows is given by Eqn. 5.

III. Domain

A. Gas Puff Valve

The Gas Puff valve has a very complex 3D geometry that makes it both difficult to model, and computationally expensive to simulate. The valve itself is composed of a central nozzle surrounded by two annular nozzles. This creates a axially symmetric geometry about the center bore of the central nozzle. Each nozzle is a supersonic converging-diverging

nozzle, the converging diverging and throat sections can be seen clearly in Fig. 1. Each nozzle is connected to a separate plenum allowing each nozzle's back pressure to be independently controlled. The separate plenum additionally allows for separate species to be fired through each nozzle, although this study will focus on homogeneous puffs.

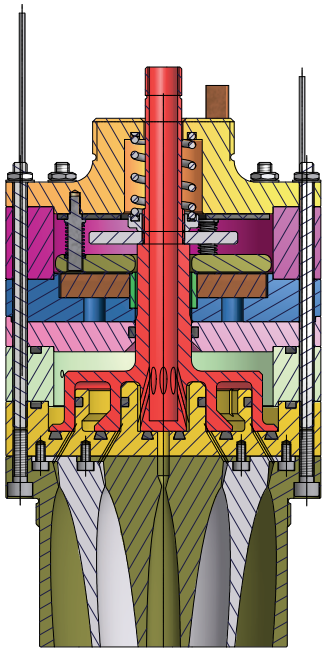

Fig. 1 Cross-sectional view of the tri-axial gas puff valve showing nozzles, plena, and valve mechanism.

B. 2D Planar Domain

As a first approximation of the complex geometry presented in Sec. III.A, a 2D planar geometry was investigated. In this domain, the complexity of the annular supersonic nozzles were eliminated by modeling the domain starting from the nozzle exits. The vacuum chamber the puff is being fired into was recreated as a rectangle with a width corresponding to the chamber diameter.

The central nozzle was placed along the horizontal at the center line or the rectangle, and two more inlets were placed at the correct heights above and below the central inlet. The distance between each inlet corresponds to the thickness of the wall between each annular nozzle. Since the actual valve is radially symmetrical, each annular nozzle corresponded to an inlet above and below the horizontal center line leading to 5 total inlets in this 2D planar case.

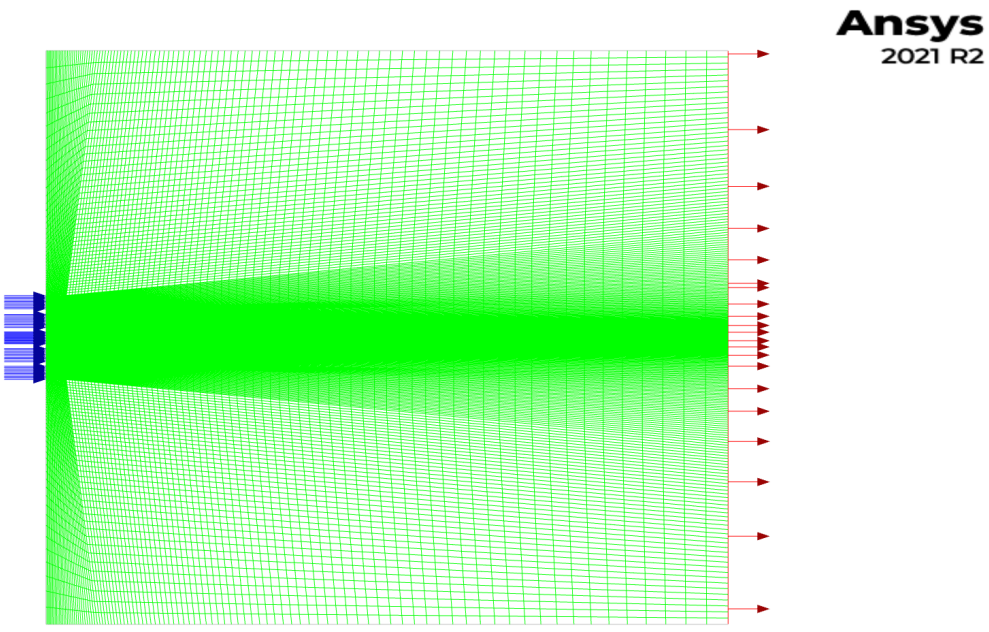

Fig. 2 Mesh and Boundary Conditions displayed for the 2D Planar Domain. Blue arrows represent inlet boundary conditions, red arrows represent outlet boundary conditions. The green lines display the mesh used for the simulation.

The upper and lower edges of the domain as seen in Fig. 2 as well as the edges on the left side of the domain not specified as an inlet were set as wall boundaries. These correspond to the vacuum chamber walls and the walls in between each of the annular nozzles. For the far edge of the domain directly opposite to the inlets, the boundary condition was set to a pressure outlet. The pressure of this boundary condition was set to the chamber pressure of 666 Pa. An outlet condition was specified at this edge of the domain for two reasons. Firstly, the length of the domain does not correspond to the length of the chamber, so the pressure outlet represents the much larger area of the vacuum chamber. The other reason is that the use of that boundary condition allows the specification of the initial pressure within the vacuum chamber at t = 0.

The inlets were all specified as pressure inlet boundary conditions. In these boundary conditions it is possible to specify both a static and total pressure quantity effectively allowing the specification of both a back pressure and a velocity. The upper most and lower most inlet conditions were paired with same initial conditions, as well as the two inlets above and below the central inlet. This reflects the fact that they do not represent individual inlets but rather two annular ring nozzles.

The mesh used for this simulation is clearly shown in Fig. 2. This mesh is densest in the region of the flow immediately surrounding the inlets. The mesh remains relatively fine with a small element size in a diverging area in front of the inlets allowing the region where most of the flow is anticipated to be to have a fine mesh. Far away from the inlets, especially close to the walls and the outlet, the mesh becomes significantly courser. This choice helped reduce the computational intensity of the simulation by reducing the detail of the simulation in areas of the domain of lower interest.

C. 2D Axisymmetric

Due to the radial symmetry of the gas puff valve, the device lends itself well to axisymmetric analysis. This model makes the same simplification of the nozzles as Sec. III.B treating the nozzle exits as pressure inlets. The stagnation pressure is once again used to specify the exit velocity of the flow leaving the nozzles.

The geometry used in the 2D axisymmetric model is similar to the that of the 2D planar case, however the domain only represents the geometry above the axis of symmetry. This can be clearly seen in Fig. 3, where the inlets lie along

the bottom edge of the domain rather than in the center. Additionally, the central inlet is only half the true width of central nozzle since the axis of symmetry is about the center bore of the central nozzle.

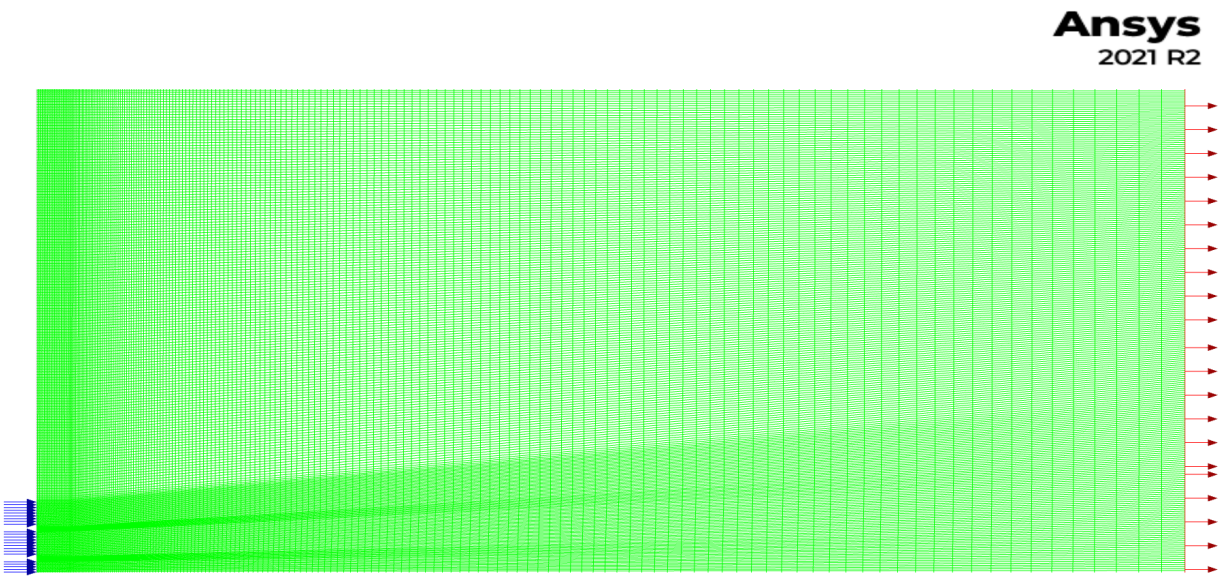

Fig. 3 Mesh and Boundary Conditions displayed for the 2D Axisymmetric Domain. Blue arrows represent inlet boundary conditions, red arrows represent outlet boundary conditions. The green lines display the mesh used for the simulation.

The only change in boundary conditions used in this simulation as compared to the one described in Sec. III.B, is the boundary condition along the bottom edge of the domain. Rather than being set to a wall boundary, it is set to an axis boundary. This informs fluent that this is the intended axis of symmetry for the simulation. The inlets and outlets are set to identical conditions as in the planar case in order to replicate the results from the first simulation.

Much like in Sec. III.B, the mesh used for the axisymmetric simulation was most fine near the inlets and along the axis of symmetry, It was coarsest by the wall and toward the outlet which were not considered areas of interest for the simulation.

IV. Results

A. 2D Planar

The first simulation carried out was with the 2D planar domain described in Sec. III.B. The domain was initialized a mixture of N_2 and O_2 based on the assumption that any residual gas in the COBRA vacuum chamber would be air. The inlet species was set to be entirely argon, with back pressures based on current COBRA pressures of interest. The central nozzle was set to 103 421 Pa (15 psi), the middle nozzle set to 14 479 Pa (2.1 psi) and the outer nozzle set to 4826.33 Pa (.7 psi). The simulation was run over a total of 500 µs of integration time with a time step of 0.05 µs corresponding with the timescale discussed in [4]. Because the nozzles of the valve were not modeled in this simulation, it was necessary to initialize the inlets with a total pressure corresponding to the velocity that the flow would have leaving the nozzles. Based on experimental work done on COBRA, it was determined that the total pressures would correspond to the fluid moving with a Mach number of 5 [4]. This allowed the calculation of total pressures to be used in Fluent and allowed the specification of an initial velocity within the pressure inlet boundary condition.

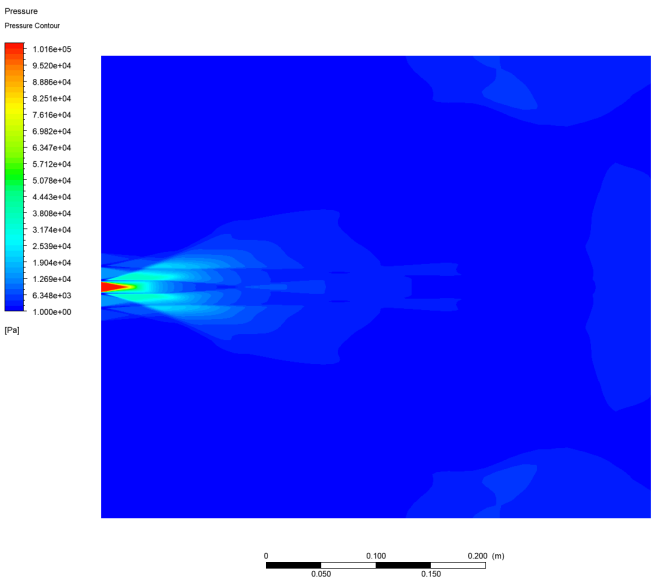

Fig. 4 Contour plot of static pressure for inlet conditions of 15:2.1:.7 psi in order of Center-Middle-Outer nozzles at time t = 500 µs

As expected the maximum pressure occurs due to the central jet which is initialized with a significantly higher pressure than the middle and outer nozzles. While the central nozzle clearly is dominating the pressure distribution, the middle and outer nozzle flows are contributing to form the structures visible in the flow in Fig. 4. It is notable that within the timescale of interest, the overall chamber pressure is not significantly affected by the puff.

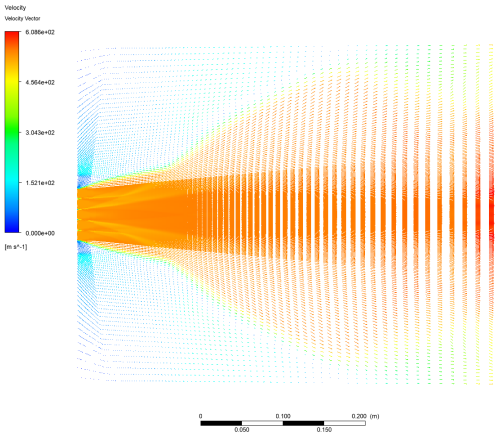

(a) Velocity Vectors for inlet conditions of 15:2.1:.7 psi in order of Center-Middle-Outer nozzles at time t = 500 µs

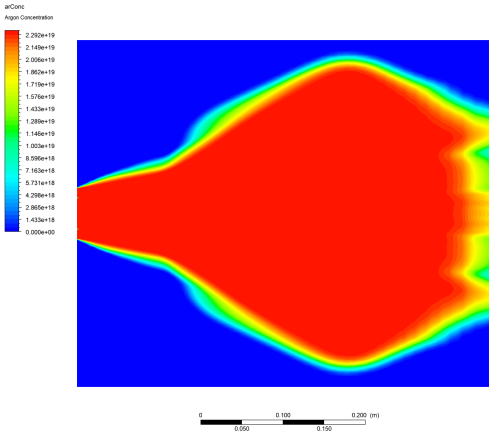

(b) Contour plot of argon number density for inlet conditions of 15:2.1:.7 psi in order of Center-Middle-Outer nozzles at time t = 500 µs

Fig. 5 Results of 2D Planar Simulation, Fig. 5a and 5b show the full simulated planar domain as described in Sec. III.B.

The number density of argon in this simulation is also interesting. The planar gas puff simulation produces a dense cloud that when close to the valve stays relatively compact, but the closer the flow is to the outlet will some what abruptly spread to the width of the chamber. It is also clear that the velocity profile of the flow shown in Fig. 5a and the argon density in Fig. 5b exhibit relatively similar general shapes. This is to be expected since the only areas that can have high speed flow must be areas with high amounts of argon since the rest of the domain is vacuum.

B. 2D Axisymmetric

The Axisymmetric simulation was initilaized with exactly the same initial conditions as the planar case described in Sec. IV.A, in order to compare between the two models. The axisymmetric case was run over the same 500 µs integration time as the previous simulation. The plots presented in Fig. 6 are mirrored across the axis of symmetry.

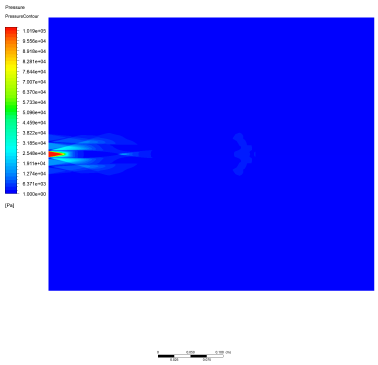

(a) Contour plot of static pressure for inlet conditions of 15:2.1:.7 psi in order of Center-Middle-Outer nozzles at time t = 500 µs

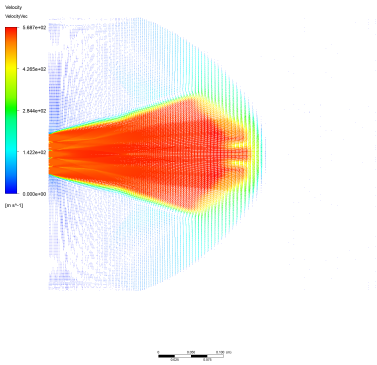

(b) Velocity Vectors for inlet conditions of 15:2.1:.7 psi in order of Center-Middle-Outer nozzles at time t = 500 µs

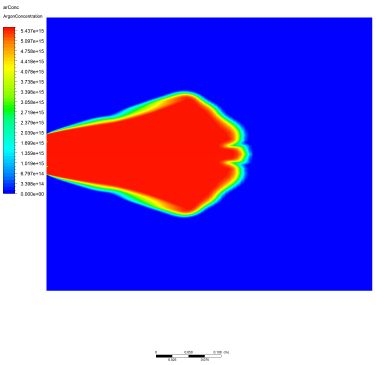

(c) Contour plot of argon number density for inlet conditions of 15:2.1:.7 psi in order of Center-Middle-Outer nozzles at time t = 500 µs

Fig. 6 Results of Axisymmetric Simulation with same initial conditions as Sec IV.A. The figures show the full domain and its reflection about the axis of symmetry.

As expected, the axisymmetric case would have significantly different results from the 2D planar case. While the planar case does resemble a slice of the gas puff valve, the planar approximation is not a particularly appropriate one. One clear indication of the difference between the axisymmetric case and the 2D planar case can be seen in Fig. 6c and Fig. 5b. The planar case has number densities that are 4 orders of magnitude greater than the in the axisymmetric case, and well above the expected number density for argon puffs within the COBRA machine [4].

The 2D planar case is best suited to flows whose domain can be extended in the out of plane direction and see very little variation. This makes the planar approximation useful for analyzing systems like flow over an airfoil, but makes it mostly inappropriate for the gas puff valve. The radial symmetry present in the device means that going into or out of the plane being investigated will change the inlet sizes or potentially hide inlets from view. Representing this system as axisymmetric does not have these same issues since the 2D plane being simulated is revolved about the plane of symmetry. The result is that the flow in the axisymmetric case has not filled the domain like in the planar case. While there are still the same structures and general shapes present in the output, as well as similar magnitudes in pressure and velocity, they are less extreme in the axisymmetric case.

C. Validation with Experimental Results

In order to investigate the validity of the axisymmetric simulation, initial conditions were set to match a test case described in 2014 paper released by LPS on the characterization of the COBRA gas puff. The paper uses plena pressures of 8 psi for the center nozzle, 3 psi for the middle and 1 psi for the outer nozzle. According to the paper, typical number density for argon of approximately 10^{17} cm^{-3} [4].

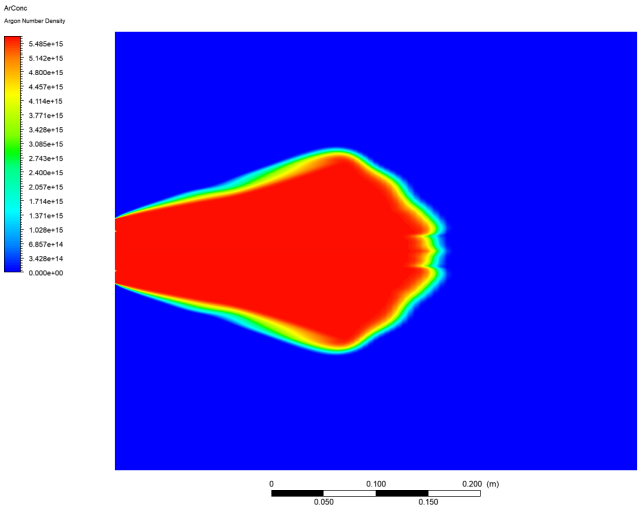

Fig. 7 Number density of argon in a gas puff with C:M:I pressures of 8:3:1 psi

As shown in Fig. 7, the simulated number density is two orders of magnitude less than is experimentally suggested. This is likely due to the averaging of mass flow rates used to calculate the number density. Additionally where the PLIF data shows three distinct puffs, in the simulation we see that the puffs blend together into one larger structure. This blending seen in the simulation likely arises from the assumptions made about the inlet pressure. In the simulation, the static pressure at the inlet is set to the static pressure in the gas puff plena, however, the pressure of the fluid as it flows through the nozzle will decrease before it reaches the chamber. This does not affect the total pressure of the flow, but a lower static pressure would likely have a significant affect on the shape of the final density profile. Correcting for this error is further discussed in Sec. V.A.

V. Conclusion

In this paper, two preliminary CFD models of the COBRA gas puff valve were developed. The first model was a 2D planar simulation that was shown to have very poor agreement with experimental data. The second model was a 2D axisymmetric model, that shows promise for being able to accurately represent the gas puffs produced in the COBRA machine. Understanding and controlling these gas puffs are critical to the study of HED Z-pinch plasmas as the density profile of the gas column is linked to the stability of the plasma. While neither simulation replicated the results of experimental work to characterize the gas puffs, they represent the first steps on a path to developing a high fidelity model.

A. Future Work

The work presented here has a number of clear extensions and next steps. One of the most significant simplifications made to the domain investigated in this paper was the elimination of the nozzle geometry. This forced the simulations to rely on total pressures in order to give the fluid velocity at the inlets. This assumes that the exit Mach number is independent of the nozzle back pressure which is not the case, and that the static pressure of the flow at the nozzle exit was equal to the plena pressure. Both of these assumptions can be eliminated through modeling of the nozzle geometry. By implementing the nozzle geometry, pressure can be specified at the nozzle inlet, where the fluid can be assumed to be approximately stationary. The large pressure gradient between the plena and the rest of the domain will be sufficient to drive the flow through the nozzle and into the chamber. This implementation will likely result in better number density predictions from the model due to a more realistic mass flow through the inlet. The first step would be to implement the nozzles into the axisymmetric model of the system. This would minimize computation time and allow for rapid validation of the model before attempting to move onto more complex formulations.

In addition to incorporating the nozzles into the axisymmetric model of the system, a full 3D simulation of the gas puff valve should be carried out. While this simulation will certainly be more computationally expensive, a full 3D model will allow for higher fidelity modeling of the gas puff and provide a better characterization of the gas puff.

Acknowledgments

I would like to acknowledge Dr. Perrine Pepiot for her support and guidance over the course of this project. Thank you for taking on this project with very little background and providing me direction throughout.

References

[1] Pereira, N. R., and Davis, J., "X rays from z-pinches on relativistic electron-beam generators," *Journal of Applied Physics*, Vol. 64, 1988, p. 1. https://doi.org/10.1063/1.341808, URL https://doi.org/10.1063/1.341808.

[2] Sze, H., Coleman, P. L., and Banister, J., "Efficient argon K-shell radiation from a Z pinch at currents >15 MA," *Physics of Plasmas*, Vol. 8, 2001, p. 3135. https://doi.org/10.1063/1.1373418, URL https://doi.org/10.1063/1.1373418.

[3] Qi, N., Rosenberg, E. W., and Gourdain, P. A., "Study of gas-puff Z-pinches on COBRA," *Phys. Plasmas*, Vol. 21, 2014, p. 112702. https://doi.org/10.1063/1.4900748, URL https://doi.org/10.1063/1.4900748.

[4] Grouchy, P. W. L. D., Rosenberg, E., and Qi, N., "Characterization of the COBRA triple-nozzle gas-puff valve using planar laser induced fluorescence," *Physics of Plasmas*, Vol. 1639, 2014, p. 112702. https://doi.org/10.1063/1.4904773, URL https://doi.org/10.1063/1.4900748.

[5] *ANSYS Fluent User's Guide*, ANSYS Inc., release 2021 r2 ed., 7 2021.

[6] *ANSYS Fluent Theory Guide*, ANSYS Inc., release 2021r2 ed., 7 2021.

[7] Donzis, D. A., Aditya, K., Sreenivasan, K. R., and Yeung, P. K., "The Turbulent Schmidt Number," *Journal of Fluids Engineering, Transactions of the ASME*, Vol. 136, 2014. https://doi.org/10.1115/1.4026619/374630, URL https://asmedigitalcollection-asme-org/fluidsengineering/article/136/6/060912/374630/The-Turbulent-Schmidt-Number.

[8] Gu, X., Yin, J., Liu, J., and Wu, Y., "A nonlinear k - ϵ turbulence model applicable to high pressure gradient and large curvature flow," *Mathematical Problems in Engineering*, Vol. 2014, 2014. https://doi.org/10.1155/2014/405202.

[9] Wilcox, D. C., "Formulation of the k-w Turbulence Model Revisited," *AIAA Journal*, Vol. 46, 2012, pp. 2823–2838. https://doi.org/10.2514/1.36541, URL https://arc.aiaa.org/doi/abs/10.2514/1.36541.

[10] Wilcox, D. C., "Reassessment of the scale-determining equation for advanced turbulence models," *AIAA Journal*, Vol. 26, 2012, pp. 1299–1310. https://doi.org/10.2514/3.10041, URL https://arc.aiaa.org/doi/abs/10.2514/3.10041.

[11] Menter, F. R., "Two-equation eddy-viscosity turbulence models for engineering applications," *AIAA Journal*, Vol. 32, 1994, pp. 1598–1605. https://doi.org/10.2514/3.12149.